

# Nonlinear FE Prediction of Shear Strength of RC T-Beams with flange in compression zone

---

**Abstract:** This research predicts the shear strength of reinforced concrete T-beams with flanges under compression stresses using nonlinear finite element (FE) analysis. A FE model is developed and verified against specially designed experiments (beams with varying flange width and depth). Results of the FE models were found to be in excellent agreement with their corresponding experimental results. The average load capacity and deflections (FE/experiments) ratios were 1.03 and 0.87, respectively. We then conducted an extensive parametric study to investigate the structural performance of flanged beams under the effect of two concentrated point loads. This parametric study examined four parameters: flange dimensions, longitudinal reinforcement in flange, concrete compressive strength, and shear span to depth ratio. Our findings indicated that the presence of compressed flanges in T-beams increases the shear strength by up to 260% of the shear strength of the web alone. The shear strength of flanged beams increases with the increase in flange dimensions, where the effect of flange thickness is more pronounced than that of flange width. Moreover, the presence of longitudinal reinforcement in the flange enhanced the beam's shear strength by up to 40%, compared to similar beams without flange reinforcement. Additionally, the shear strength increased up to three-fold for various beam conditions when the shear span to depth ratio was reduced from 2.0 to 0.5. These findings provide valuable insights for designing and constructing reinforced concrete T-beams with flanges under compression stresses.

**Keywords:** *finite element analysis, shear strength, reinforced concrete beams, T-beam, Girder.*

---

---

## 1. INTRODUCTION

Flanged reinforced concrete beams have been widely used in many applications in the field of civil engineering. As such, the performance of these structural members was discussed experimentally as well as analytically. Hesham et al. [2] conducted a numerical experimental study the shear behavior of lightweight concrete flanged beams. Six lightweight concrete beams were tested to investigate the effects of flange width and shear span to depth ratio. Their experimental and FE results showed that the failure load of T-beams with different flange widths (320, 520, and 720 mm) increased in proportion to the flange width. However, it was also observed that the failure load was inversely proportional to all the shear span to depth ratio.

41 Balamuralikrishnan et al. [3] performed experiments as well as FE investigations to evaluate the  
42 performance of RC T-beams reinforced internally with GFRP reinforcements to shearing loads. A total  
43 of twelve specimens were tested with varying parameters (type of reinforcements, reinforcements ratio,  
44 and concrete grade). Finite element modeling of the T- beams was done using ANSYS program utilizing  
45 two special elements: solid 65 and link 8. The experimental outcomes of the flanged beams agreed well  
46 with the FE numerical results.

47 Hamdy et al. [4] showed that finite element modeling via ANSYS program was able to fairly predict  
48 the performance of RC T-beams with openings reinforced with either carbon fiber reinforced polymer  
49 (CFRP) or basalt fiber reinforced polymer (BFRP) sheets. In particular, ANSYS finite element models  
50 could reasonably predict the failure load and the mode of failure for the analyzed beams.

51 Hugo et al. [5] pointed out that the serviceability circumstances of T-beams can be improved by  
52 increasing the concrete strengths as concrete strength has an essential influence on the de-bonding  
53 phenomenon.

54 Pansuk et al. [6] indicated that an increase in the flange width of a T-beam gave higher shear capacity  
55 (in a nonlinear relationship) for the T-beams with shear reinforcement. However, they found that in the  
56 case of a T-beam without shear reinforcement, the width of the flange has almost no effect on shear  
57 capacity.

58 Sato et al. [7] showed that concrete top flanges had significant effects on shear behavior of RC T-  
59 beams as it affects the shear strength, stress in shear reinforcement, and crack propagation. Concrete  
60 top flanges could also reduce the shear strains in the beam web. They recommended that concrete top  
61 flange near compression zone should be considered as part of the shear resisting mechanism of T-  
62 beams.

63 Finally, Giaccio et al. [8] tested fifteen flanged specimens with shear reinforcement and web  
64 longitudinal reinforcement. There observed the effect of the flange width to web width ratio ( $b_f/b_w$ ) on  
65 the shear strength of reinforced concrete T-beams; this effect depended on the ratio of flange thickness  
66 to effective beam depth ( $d_f/d_o$ ). They suggested based on their experiments that as long as the ratio  
67  $d_f/d_o$  is above a certain minimum value ( $d_f/d_o \geq 0.25$ ), then the increase in shear resistance for a given  
68 increase in  $b_f/b_w$  is independent of  $d_f/d_o$ .

69 Numerical analysis technique that is based on the finite element method has been checked in this  
70 research to detect the effect of the flange on the reinforced concrete T-beams in both pre- and post-

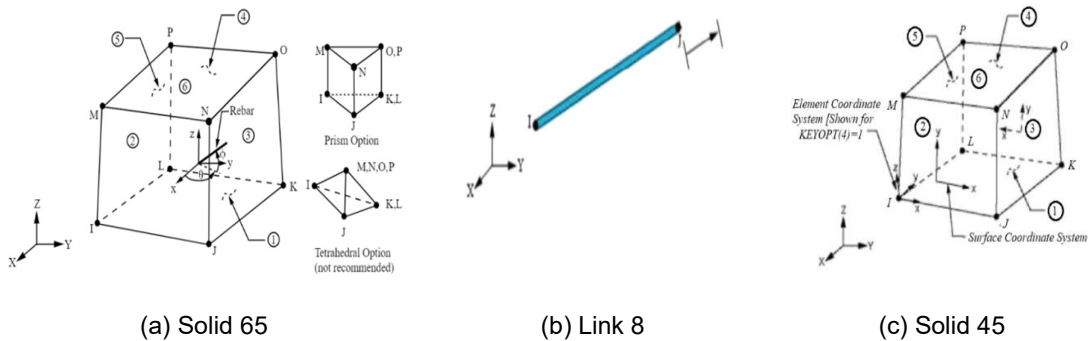
71 cracking stages of loading and up to ultimate load. ANSYS [1] is adopted in the study as it is furnished  
 72 with sufficient modelling features that suit the finite element analysis of RC beams. First, 3-D nonlinear  
 73 FE models of flanged beams "**with flange in the compression**" were specially developed using  
 74 ANSYS V-19.2. Then, results obtained were validated through comparisons with the test results of  
 75 specially designed and conducted experiments that included similar beams. Results of the FE models  
 76 agreed very well with **the** corresponding experimental results; the theoretical and experimental crack  
 77 patterns were also in good practical agreement. Using this validated model, it was possible to run an  
 78 extensive parametric study of all variables, a study that couldn't be done experimentally due to cost and  
 79 time constraints.

## 80 2. FINITE ELEMENT MODELING USING ANSYS

### 81 2.1. Geometry

82 Finite element modeling and nonlinear analysis are performed using ANSYS software. The structural  
 83 element types adopted for geometric idealization of the different materials are SOLID 65 for concrete,  
 84 and LINK 8 for steel bars and stirrups. In order to avoid stress concentration problems such as localized  
 85 crushing of concrete elements near the bearing and loading plates, SOLID 45 elements are used to  
 86 model the 30 mm thickness steel plates inserted at locations of supports and concentrated loads (see  
 87 Fig. 1 for modelling layout). For solving the nonlinear equations using Newton- Raphson equilibrium  
 88 iteration technique, the infinite norm of displacement and the convergence precision are taken equal to  
 89 0.05 [9,10,11]. Figure 2 shows the loading configuration and support conditions.

90



91 **Fig. 1** Structural elements idealization for the numerical models [9].

92

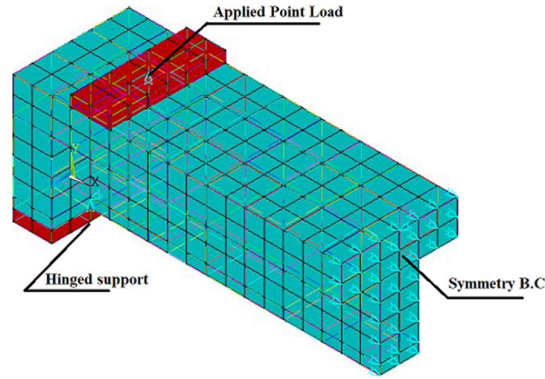


Fig. 2 Applied Load and Support Conditions.

93

## 2.2. Constitutive Relations

94

95 Constitutive relationships for both the reinforcement and the concrete are described below.

96

### 2.2.1. Constitutive relation for concrete

97

98 Concrete is a quasi-brittle material that behaves differently in compression and tension. The tensile  
99 strength of concrete is typically 8-15% of its compressive strength [12]. Figure 3 shows a typical stress-  
strain curve for normal weight concrete applied in our numerical study [13].

100

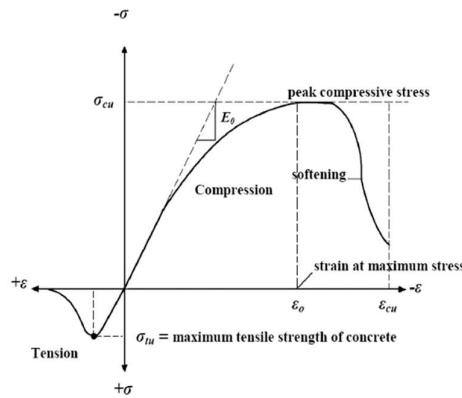


Fig. 3 Typical uniaxial compressive and tensile stress-strain curve for concrete (Bangash1989)

101

102 To define concrete material in ANSYS, the following inputs are required: elastic modulus ( $E_c$ ); ultimate  
103 uniaxial compressive strength ( $f'_c$ ); ultimate uniaxial tensile strength (modulus of rupture,  $f_r$ ); Poisson's  
104 ratio ( $\nu$ ); and shear transfer coefficient ( $\beta_t$ ). To define the uniaxial stress-strain relationship for concrete  
105 in compression, Eqs. 1 to 3 were used [14].

106

$$f = \frac{E_c \varepsilon}{1 + \left(\frac{\varepsilon}{\varepsilon_o}\right)^2} \quad (1)$$

107 
$$\epsilon_o = \frac{2f_c'}{E_c} \quad (2)$$

108 
$$E_c = \frac{f}{\epsilon} \quad (3)$$

109 Where:

110  $f$  = stress at any strain  $\epsilon$ , psi

111  $\epsilon$  = strain at stress  $f$

112  $\epsilon_o$  = strain at the ultimate compressive strength  $f_c'$

113  $E_c$  = the initial tangent modulus for concrete in MPa and is defined according to ACI-318 14 [17] by the following equations:

115

116 
$$E_c = 4700 \sqrt{f_c'} \quad (4)$$

117 Figure 4 shows the simplified compressive uniaxial stress-strain relationship adopted in this study.

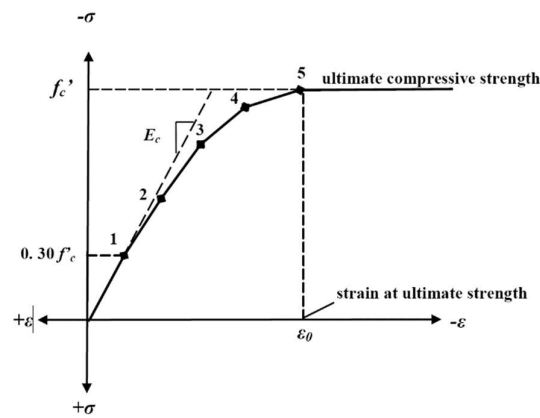


Fig. 4 Simplified compressive uniaxial stress-strain curve for concrete

118

### 2.2.2. Constitutive relation for steel

119

120 Figure 5 shows the idealized stress-strain relationship for the steel reinforcement. Material properties

121 are as follows: elastic modulus,  $E_s=200,000$  MPa; yield stress,  $f_y = 420$  MPa (Lab test); and Poisson's

122 ratio,  $\nu = 0.3$ .

123

124

125

126

127

128

129

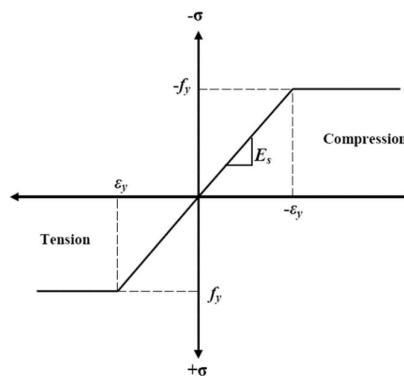
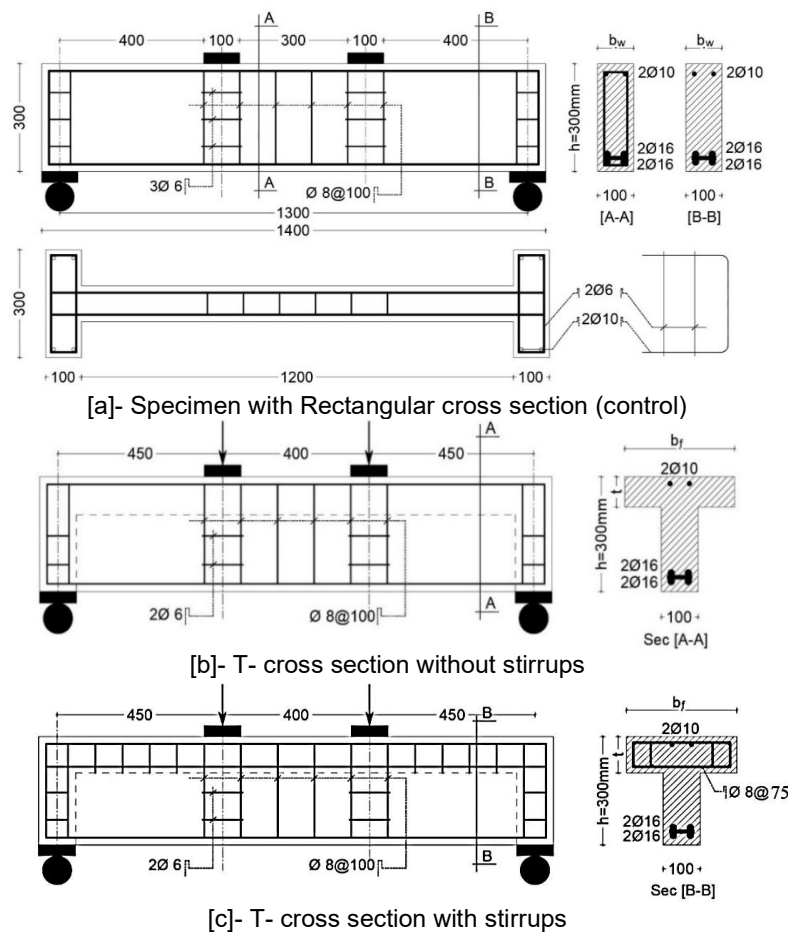


Fig. 5 Idealized stress-strain curve for reinforcing steel

130 **3. MODEL VALIDATION**

131 In this section, results of the FE model are validated using test results of a recent experimental  
 132 investigation conducted by the authors [16]. Table 1 presents the geometrical and mechanical  
 133 properties of few selected specimens for comparison. Furthermore, the test set-up together with  
 134 specimens' details are shown in Figures 6 and 7, respectively, while the corresponding finite element  
 135 models are shown in Fig. 8. For details about the full experimental program to nineteen specimens,  
 136 please refer to [16].



137 **Fig. 6** Specimen details and arrangement of reinforcement (All dimensions in mm) [16]

138

139

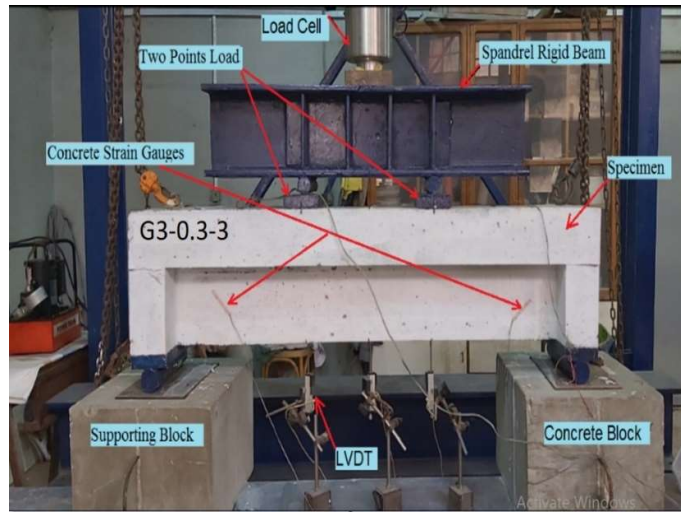
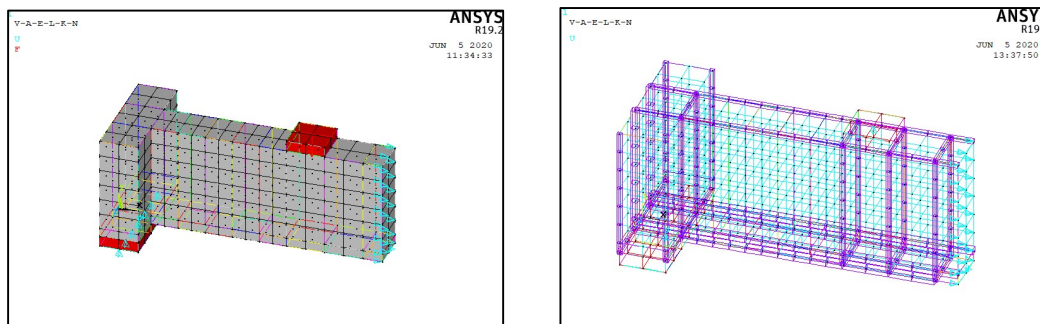


Fig. 7 Preparation of Test Set-up Specimens [16]

Table-1 Experimental Program

Specimen	Cross Sectional Area (cm <sup>2</sup> )	Cross Sectional Area Increasing (%)	Flange Dim.			Stirrups in flange within shear zone (mm)	Longitudinal reinforcement in Flange		Longitudinal reinforcement in Flange [%]
			$t_f$ (cm)	$b_f$ (cm)	$A_f$ (cm <sup>2</sup> )		Bottom Steel	Top Steel	
C0	300	-----							
G1-0.3-3	480	60%	0.3h= 9	30	270	-----			
G3-0.5-5	900	200%	0.5h=15	50	750	Ø8@75	6 Ø 10 + 1Ø10/side	2 Ø 8 + 2 Ø 6	1.046%

For specimens G1-0.3-3 and G3-0.5-5: the first part G1 refers to without flange reinforcement while G3 with longitudinal bars and flange stirrups within the shear zones; the second part refers to the ratio of flange thickness to the total depth ( $\rho_t = 0.3$  and  $0.5$ ); and the third part refers to the flange width to web width ratio ( $\rho_b = 3$  and  $5$ ).



(a)

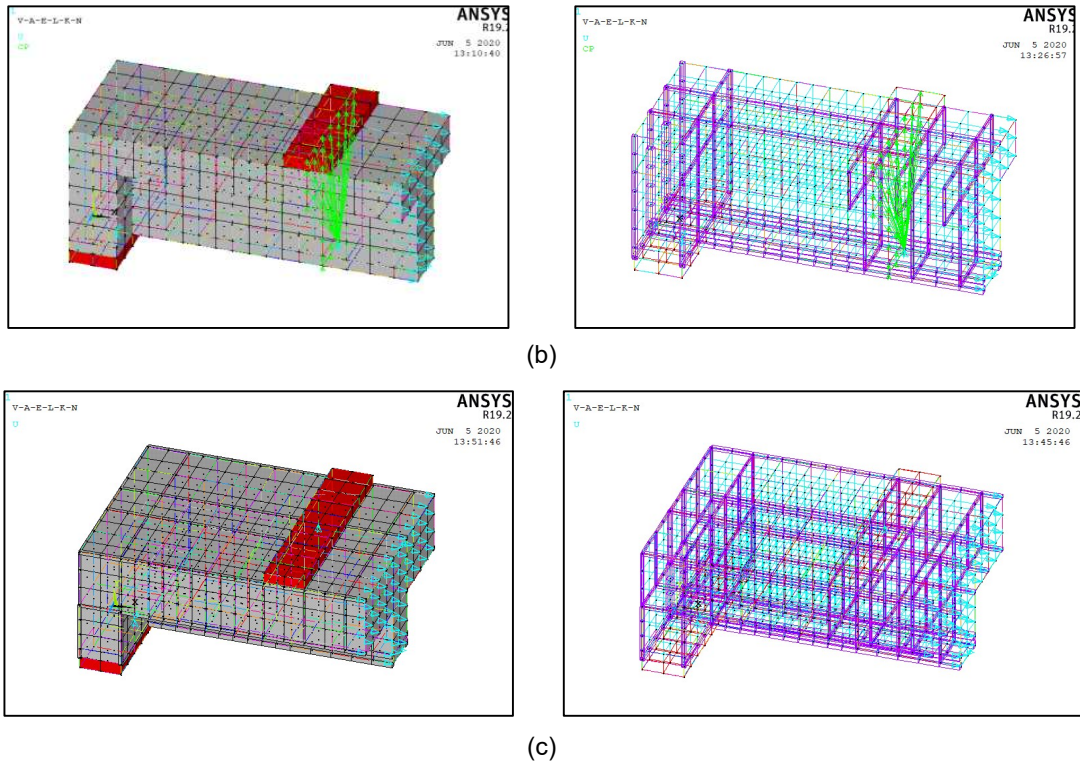


**Fig. 8** Finite Element Simulation Models for specimens: a) Rectangular; b) G1-0.3-3; and c) G3-0.5-5 from Ref. [16]

141 **3.1. Load deflection curves**

142 Figure 9 compares the load-deflection calculated using ANSYS models with the corresponding  
 143 experimental measurements for three specimens (C0, G1-0.3-3 & G3-0.5-5). It is seen that the FE  
 144 results agree very well with the experiments [16] in terms of the ultimate load capacity ( $P_u$ ) and the  
 145 corresponding ultimate deflection ( $\Delta_u$ ). It is noted, however, that- in the initial part- the theoretical load-  
 146 deflection curve is 9% to 15% stiffer than that obtained experimentally. Besides, the average ratio of  
 147 FE to experimental ultimate deflections [ $\Delta_{u(FE)}/\Delta_{u(EXP)}$ ] for all specimens was 0.87.

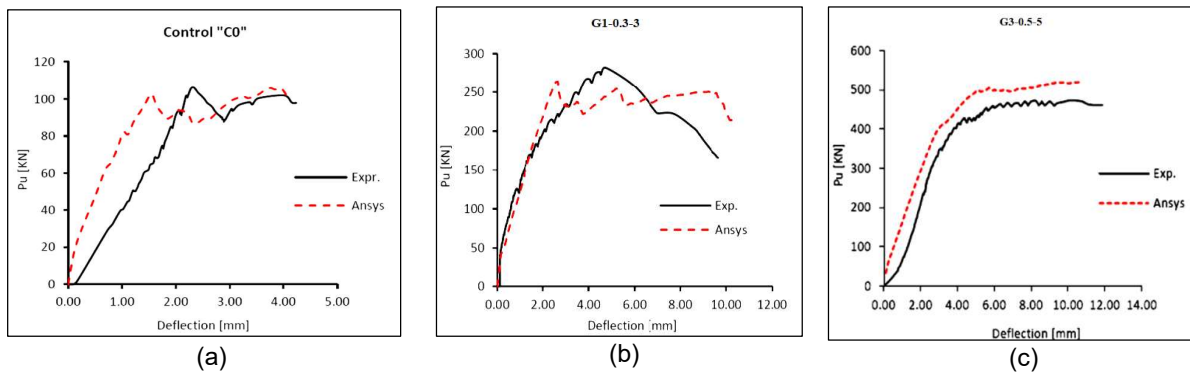


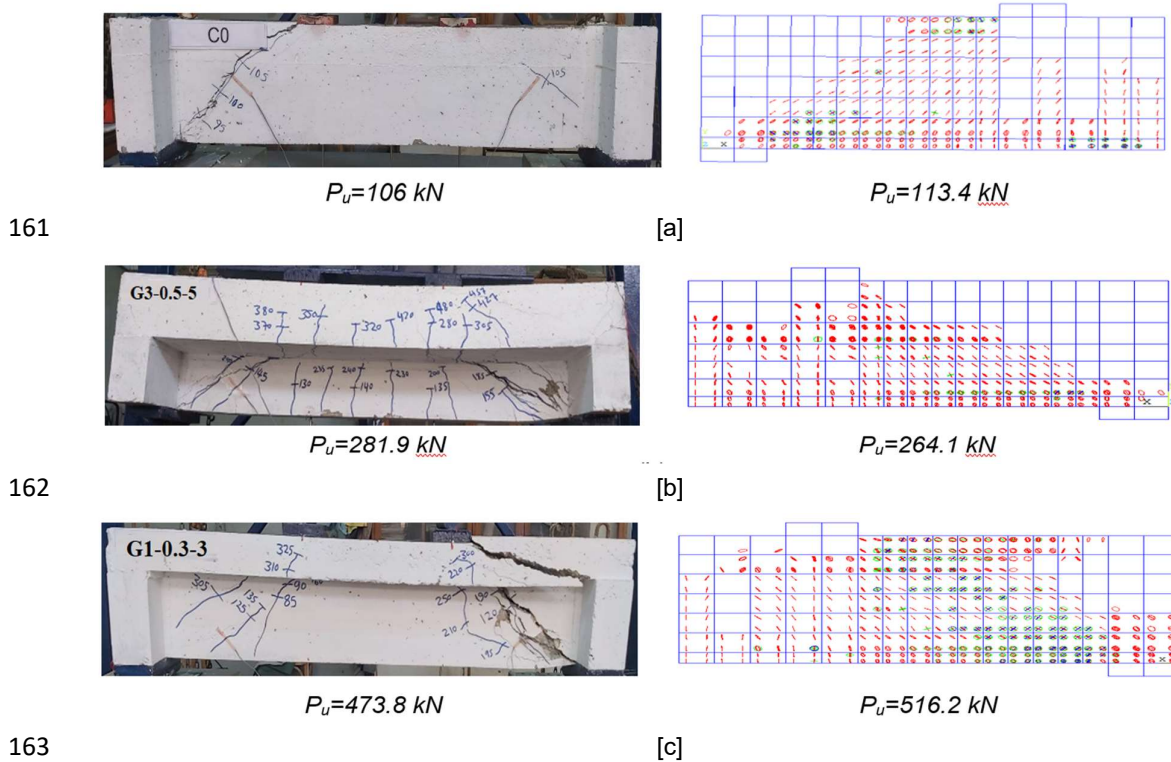
**Fig.9** Predicted and Measured Load-Deflections Curves for Three Specimens: a) Rectangular; b) G1-0.3-3; and c) G3-0.5-5. [16]

148 **3.2. Ultimate load comparison**

149 The experimental ultimate loads for specimens C0, G1-0.3-3, and G3-0.5-5 were  
150 106.4, 281.9, and 473.8 kN; respectively; while its FE predictions were 113.4, 264.1,  
151 and 516.2 kN; respectively. The difference between the theoretical and experimental  
152 ultimate loads is about  $\pm 6\%$ , while the average of the  $[P_{U(FE)} / P_{U(EXP)}]$  ratio for all  
153 specimens is 1.03. This validates accuracy of the ANSYS model and qualifies it for  
154 use in the parametric study to examine the performance of reinforced concrete T-  
155 beams.

156 **3.3. Crack pattern and failure mode**

157 A comparison between the experimental crack patterns for tested beams in Ref. [16] with the predicted  
158 crack patterns by ANSYS is shown in Fig. 10. All specimens failed in shear (mode) distinguished by  
159 wide diagonal cracks extending from close to the supporting column towards the steel loading plate. In  
160 addition, the figure shows change in spreading of cracks with the presence and size of flange.



164 **Fig. 10** Predicted and Observed Cracking Patterns and Failure Load for Three Specimens: a)  
165 Rectangular; b) G1-0.3s-3; and c) G3-0.5-5 [16].

166 **Parametric study.**

167 **3.4. General**

168 **In order to** study the effect of different parameters on the structural response of RC T-beams,  
 169 several beams (labeled as S, S1, S2, ... S96) are analyzed. As given in Table 2, the main  
 170 considered parameters include: (1) the concrete strength ( $f_c'$ ), (2) width ratio ( $\rho_b$ ), (3) depth  
 171 ratio ( $\rho_t$ ), (4) ratio of longitudinal steel in flange ( $\rho$ ), and (5) shear span to depth ratio ( $a/d$ ).  
 172 The rectangular beam S is the reference or control case.

**Table 2** Parametric Study

Specimen	width ratio ( $\rho_b$ )	depth ratio ( $\rho_t$ )	$a/d$	$f_c'$	Longitudinal steel in flange $\rho$ %	No of Runs
S	-----	-----	2.0	30	-----	1
S 1:12	3	0.10, 0.3, 0.5& 0.7	0.5, 1.0, and 2.0	30	0.5	12
S 13:24	5	0.10, 0.3, 0.5& 0.7	0.5, 1.0, and 2.0	30	0.5	12
S 25:48	7	0.10, 0.3, 0.5& 0.7	0.5, 1.0, and 2.0	30 and 60	0.5	24
S 49:84	7	0.10, 0.3, 0.5& 0.7	0.5, 1.0, and 2.0	30	0.0, 1.0, and 2.0	36
S 85:96	9	0.10, 0.3, 0.5& 0.7	0.5, 1.0, and 2.0	30	0.5	12
Total						97

Width ratio ( $\rho_b = b_f/b_w$ ) is the ratio of flange width “ $b_f$ ” and web width “ $b_w$ ”, depth ratio ( $\rho_t = t/h$ ) is the ratio of flange thickness “ $t$ ” and total web depth “ $h$ ”,  $a/d$  is the span to depth ratio,  $\rho$  % is the longitudinal steel in the flange. Control specimen S is rectangular section, with total depth 300 mm and width 100 mm.

173  
 174 **Note:** In every row of Table 2, as the beam label increases (from  $S_i$  to  $S_{i+1}$ ,  $S_{i+2}$ , etc.) changes in  
 175 parameters occur first for  $\rho_t$ , then for  $a/d$ , then for  $f_c'$ , and finally for  $\rho$ , as listed in the table. Thus, S49  
 176 designates the beam with  $\rho_t = 0.1$ ,  $a/d = 0.5$ , and  $\rho = 0.0$ , while S54 represents the beam with  $\rho_t = 0.3$ ,  
 177  $a/d = 1.0$ , and  $\rho = 0.0$ , and S79 is the beam with  $\rho_t = 0.5$ ,  $a/d = 1.0$ , and  $\rho = 2.0$ .

178 **3.5. Presentation of ANSYS results**

179 The following terms were used to present the results and all specimens' results are displayed in  
 180 **Table 3.**

- 181 ▪ Loads at the yield level ( $P_y$ ) and at the ultimate level ( $P_u$ ).
- 182 ▪ Deflection at the yield level ( $\Delta_y$ ) and at the ultimate level ( $\Delta_u$ ).
- 183 ▪ Displacement ductility ( $\mu_\Delta$ ) = ( $\Delta_u/\Delta_y$ ).
- 184 ▪ Toughness (I) = the area under the load-deflection curve.

185

**Table 3** Numerical results for various analyzed beams

Specimen	$P_u$ (kN)	$P_y$ (kN)	$P_{cr}$ (kN)	$\Delta_u$ (mm)	$\Delta_y$ (mm)	$\Delta_{cr}$ (mm)	$Q_{uR}$	$\alpha_{uR}$	$l$	$l_{uR}$
S	141.61	-----	33.47	2.81	-----	0.34	1	1	1089	1.0
S1	559.50	356.40	140.44	2.86	3.03	0.36	3.95	1.02	2907	2.7
S2	516.96	437.77	142.56	2.04	2.51	0.33	3.65	0.73	3846	3.5
S3	692.85	430.30	150.87	2.91	3.18	0.38	4.89	1.04	3673	3.4
S4	714.67	N.Y*	178.62	2.43	N.Y*	0.38	5.05	0.86	4364	4.0
S5	300.22	210.57	72.36	2.53	2.82	0.38	2.12	0.90	1717	1.6
S6	328.58	271.78	72.66	2.67	3.53	0.33	2.32	0.95	2715	2.5
S7	440.19	427.09	73.28	3.92	4.21	0.34	3.11	1.40	3104	2.9
S8	500.99	N.Y	86.67	3.65	N.Y	0.33	3.54	1.30	3119	2.9
S9	156.09	100.52	38.30	2.69	7.35	0.32	1.10	0.96	1022	0.9
S10	198.57	147.53	35.73	3.57	5.05	0.27	1.40	1.27	1446	1.3
S11	270.99	195.03	37.47	4.50	5.37	0.27	1.91	1.60	1674	1.5
S12	354.17	N.Y	45.78	5.13	N.Y	0.29	2.50	1.83	2127	2.0
S13	572.64	560.06	148.62	2.54	2.56	0.38	4.04	0.90	3088	2.8
S14	623.87	621.41	157.71	2.93	2.90	0.37	4.41	1.04	4861	4.5
S15	769.96	756.27	168.70	2.75	3.50	0.40	5.44	0.98	6633	6.1
S16	882.42	N.Y	218.41	2.86	N.Y	0.34	6.23	1.02	6909	6.3
S17	284.25	193.88	71.34	2.35	4.11	0.33	2.01	0.84	1883	1.7
S18	361.60	282.53	73.14	2.70	3.72	0.32	2.55	0.96	2871	2.6
S19	520.52	492.87	80.92	4.67	5.07	0.33	3.68	1.66	4373	4.0
S20	651.44	N.Y	110.52	4.23	N.Y	0.33	4.60	1.51	4493	4.1
S21	155.06	98.58	34.58	4.24	6.02	0.23	1.09	1.51	1087	1.0
S22	205.31	172.54	38.04	3.23	6.78	0.30	1.45	1.15	1540	1.4
S23	291.47	253.38	43.59	4.14	5.38	0.23	2.06	1.47	2194	2.0
S24	437.37	422.75	59.74	5.62	5.01	0.29	3.09	2.00	3605	3.3
S25	539.03	450.27	147.13	2.50	1.55	0.36	3.81	0.89	4428	4.1
S26	601.13	555.55	155.19	2.03	2.28	0.36	4.24	0.72	5587	5.1
S27	813.05	598.64	186.74	2.41	4.57	0.37	5.74	0.86	6426	5.9
S28	955.33	N.Y	266.28	2.51	N.Y	0.35	6.75	0.89	6911	6.3
S29	291.17	206.89	75.67	2.16	3.73	0.32	2.06	0.77	2055	1.9
S30	370.20	340.28	76.91	2.53	4.11	0.31	2.61	0.90	3413	3.1
S31	583.19	432.66	89.37	3.64	4.33	0.31	4.12	1.29	4434	4.1
S32	683.84	N.Y	140.99	3.85	N.Y	0.33	4.97	1.37	5042	4.6
S33	155.33	142.38	40.71	2.58	5.27	0.28	1.10	0.92	1172	1.1
S34	216.92	162.65	43.43	3.07	6.90	0.23	1.53	1.09	1683	1.5
S35	345.30	N.Y	48.58	4.41	N.Y	0.26	2.44	1.57	2678	2.5
S36	468.64	N.Y	73.43	4.76	N.Y	0.28	3.31	1.69	3403	3.1
S37	966.03	780.48	184.95	3.21	3.44	0.29	6.82	1.14	8841	8.1
S38	1160.45	1091.52	190.97	4.03	3.66	0.30	8.19	1.43	10419	9.6
S39	1616.71	1488.36	225.87	11.42	5.14	0.33	11.42	4.06	16049	14.7
S40	1575.32	1409.87	337.32	4.47	8.56	0.33	11.12	1.59	12934	11.9
S41	537.98	457.99	88.35	3.81	5.05	0.33	3.80	1.35	4829	4.4
S42	729.11	674.25	94.84	15.30	7.70	0.31	5.15	5.44	9242	8.5
S43	899.35	830.58	113.21	17.34	6.49	0.31	6.35	6.17	13217	12.1
S44	1089.80	1010.36	178.46	12.49	5.27	0.33	7.70	4.44	14311	13.1
S45	291.42	258.80	43.89	5.41	7.07	0.27	2.06	1.93	2239	2.1

<i>Specimen</i>	$P_u$ (kN)	$P_y$ (kN)	$P_{cr}$ (kN)	$\Delta_u$ (mm)	$\Delta_y$ (mm)	$\Delta_{cr}$ (mm)	$Q_{uR}$	$a_{uR}$	$I$	$I_{uR}$
S46	387.44	362.88	46.12	11.57	6.76	0.26	2.74	4.12	3544	3.3
S47	471.56	420.76	57.63	11.46	5.11	0.26	3.33	4.08	4526	4.2
S48	594.53	515.21	93.98	12.00	4.23	0.28	4.20	4.27	5637	5.2
S49	552.96	N.Y	141.13	2.34	N.Y	0.33	3.90	0.83	4069	3.7
S50	618.56	N.Y	155.58	2.23	N.Y	0.29	4.37	0.80	5694	5.2
S51	772.52	N.Y	157.25	2.73	N.Y	0.25	5.46	0.97	5932	5.4
S52	831.80	N.Y	184.54	2.95	N.Y	0.24	5.87	1.05	7118	6.5
S53	305.85	N.Y	102.28	2.40	N.Y	0.60	2.16	0.85	2832	2.6
S54	340.13	N.Y	76.79	2.35	N.Y	0.31	2.40	0.84	1628	1.5
S55	456.24	N.Y	87.24	3.21	N.Y	0.30	3.22	1.14	3252	3.0
S56	648.25	N.Y	135.01	5.25	N.Y	0.35	4.58	1.87	5316	4.9
S57	161.20	N.Y	37.59	2.66	N.Y	0.27	1.14	0.95	1086	1.0
S58	229.81	N.Y	39.64	3.93	N.Y	0.27	1.62	1.40	1591	1.5
S59	310.08	N.Y	46.74	5.56	N.Y	0.27	2.19	1.98	2277	2.1
S60	336.09	N.Y	65.19	6.74	N.Y	0.26	2.37	2.40	3019	2.8
S61	545.20	435.37	146.33	2.21	9.09	0.36	3.85	0.79	4563	4.2
S62	673.43	N.Y	159.83	2.25	N.Y	0.39	4.76	0.80	5696	5.2
S63	839.89	N.Y	188.97	2.51	N.Y	0.33	5.93	0.89	6190	5.7
S64	972.73	N.Y	254.32	2.45	N.Y	0.31	6.94	0.87	8186	7.5
S65	319.21	216.90	78.21	2.47	9.33	0.37	2.25	0.88	2430	2.2
S66	418.11	N.Y	83.40	3.02	N.Y	0.37	2.95	1.07	3392	3.1
S67	610.65	N.Y	91.59	4.44	N.Y	0.30	4.31	1.58	5294	4.9
S68	703.74	N.Y	151.69	3.51	N.Y	0.34	4.83	1.25	5627	5.2
S69	155.78	N.Y	40.91	2.50	N.Y	0.28	1.10	0.89	1139	1.0
S70	246.86	N.Y	38.21	3.84	N.Y	0.25	1.74	1.37	2008	1.8
S71	433.35	N.Y	49.18	6.42	N.Y	0.26	3.06	2.28	3222	3.0
S72	460.77	N.Y	82.91	4.61	N.Y	0.30	3.25	1.64	3440	3.2
S73	564.70	N.Y	147.63	2.55	N.Y	0.36	3.99	0.91	4697	4.3
S74	744.36	N.Y	153.98	2.94	N.Y	0.31	5.26	1.05	5158	4.7
S75	853.55	N.Y	196.26	2.37	N.Y	0.32	6.03	0.84	6025	5.5
S76	982.97	N.Y	295.72	4.54	N.Y	0.35	6.87	1.62	8148	7.5
S77	325.30	N.Y	72.43	2.63	N.Y	0.32	2.30	0.94	2289	2.1
S78	396.49	N.Y	77.21	2.70	N.Y	0.31	2.80	0.96	3879	3.6
S79	574.60	N.Y	99.76	3.09	N.Y	0.32	4.06	1.10	4708	4.3
S80	690.89	N.Y	160.98	3.47	N.Y	0.34	4.88	1.24	5451	5.0
S81	169.86	N.Y	38.23	3.02	N.Y	0.27	1.20	1.07	1317	1.2
S82	260.72	N.Y	39.36	4.61	N.Y	0.27	1.84	1.64	2169	2.0
S83	401.81	N.Y	51.43	4.20	N.Y	0.26	2.84	1.50	2647	2.4
S84	473.23	N.Y	87.67	4.94	N.Y	0.29	3.34	1.76	3589	3.3
S85	552.58	N.Y	143.38	2.30	N.Y	0.32	3.90	0.82	3252	3.0
S86	657.33	N.Y	159.68	6.30	N.Y	0.29	4.64	2.24	5226	4.8
S87	855.04	N.Y	211.25	5.43	N.Y	0.36	6.04	1.93	4052	3.7
S88	1091.01	N.Y	262.26	3.22	N.Y	0.29	7.70	1.15	4738	4.4
S89	307.32	192.59	76.99	2.40	4.66	0.3217	2.17	0.85	2017	1.9
S90	406.85	381.67	84.37	2.75	4.01	0.31	2.87	0.98	3574	3.3
S91	613.52	462.25	102.29	3.70	4.40	0.32	4.33	1.32	4266	3.9
S92	690.99	N.Y	164.68	3.37	N.Y	0.33	4.88	1.20	6088	5.6

Specimen	$P_u$ (kN)	$P_y$ (kN)	$P_{cr}$ (kN)	$\Delta_u$ (mm)	$\Delta_y$ (mm)	$\Delta_{cr}$ (mm)	$Q_{uR}$	$\alpha_{uR}$	$I$	$I_{uR}$
S93	159.26	129.55	37.48	2.73	7.28	0.27	1.12	0.97	1203	1.1
S94	247.99	192.69	41.81	3.78	6.50	0.27	1.75	1.34	1920	1.8
S95	389.48	302.82	53.68	5.79	8.00	0.26	2.75	2.06	2914	2.7
S96	512.85	N.Y	85.62	5.08	N.Y	0.28	3.62	1.81	2074	1.9

187 \* : The longitudinal steel in flange Did Not Yield

188 Where:

$$Q_{uR} = \text{Shear capacity ratio at the ultimate load level} = P_u / P_{ur} \quad (5)$$

$$\alpha_{uR} = \text{Deflection ratio at the ultimate load level} = \Delta_u / \Delta_{ur} \quad (7)$$

$$I_{uR} = \text{Toughness ratio} = I / I_{ur} \quad (8)$$

189 And

$P_{cr}$  : Cracked load (kN). 190

$\Delta_{cr}$  : The deflection at the first crack (mm). 191

$P_{ur}$  : Shear capacity at the ultimate load level for the control specimen (S). 192

$\Delta_{ur}$  : Deflection at the ultimate level for the control specimen. 193

$I_{ur}$  : Toughness of the control specimen. 193

194 **3.6. Effect of flange dimensions: width ratio ( $\rho_b = b_f / b_w$ ) and depth ratio ( $\rho_t = t/h$ )**

195 Figure 11 presents the variation of beam ultimate shear strength,  $P_u$ , with the flange width ratio ( $\rho_b$ )  
196 for T-beams with variable flange thickness ratio ( $\rho_t$ ). In addition, Fig. 12 presents the variation of beam  
197 ultimate shear strength,  $P_u$ , with the flange thickness ratio ( $\rho_t$ ) for T-beams with variable flange width  
198 ratio ( $\rho_b$ ). The data in Figs. 11 and 12 corresponds to beams with  $\rho = 0.5$ ,  $f_c' = 30$ , and  $a/h = 2$ . Compared  
199 to control beam S (with  $P_u = 141.61$  kN), presence of flange with a width of triple times web width ( $\rho_b =$   
200 3) and with thickness of 0.1, 0.3, 0.5, and 0.7 of beam depth; increased beam shear strength  $P_u$  by  
201 10%, 40%, 90%, and 150%; respectively. Besides, for flange width of nine times web width ( $\rho_b = 9$ ), the  
202 corresponding increases in beam shear strength become 12%, 75%, 175%, and 260%; respectively.  
203 Both flange width and thickness affect the shear strength of T-beams while the effect of flange thickness  
204 is more pronounced. For thin flanges ( $\rho_t = 0.10$ ), increasing flange width does not help.

205

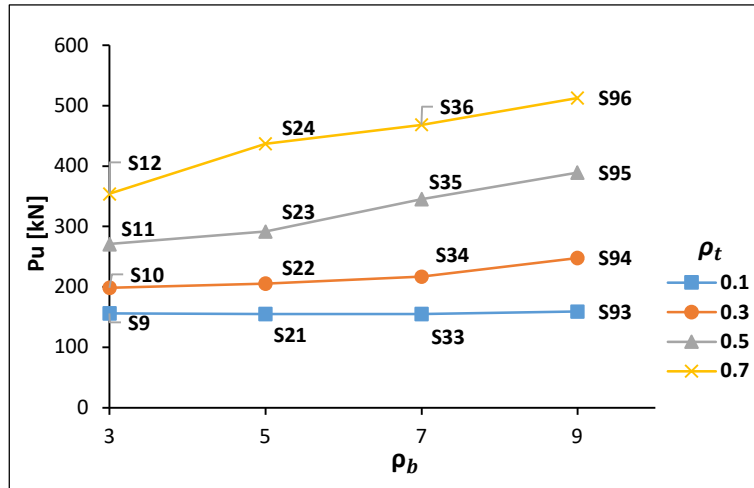


Fig. 11 Variation of ultimate load  $P_u$  with flange width ratio ( $\rho_b$ ) at different flange thickness ratios ( $\rho_t$ ) for  $\rho = 0.5$ ,  $f_c' = 30$  MPa &  $a/h = 2$ .

206

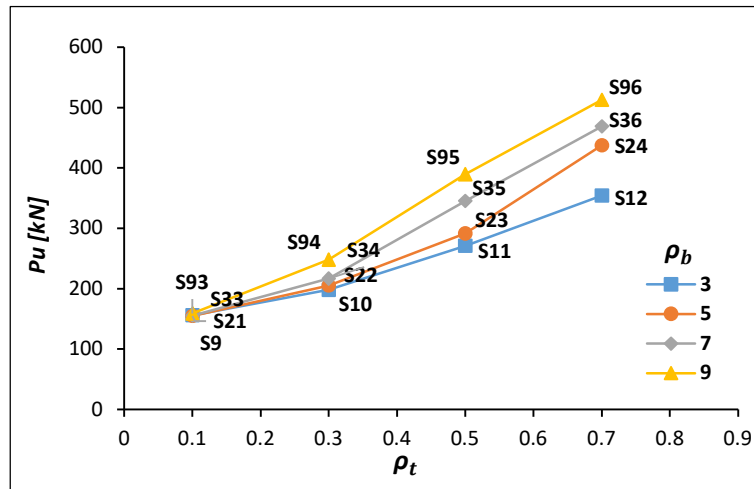


Fig. 12 Variation of ultimate load  $P_u$  with flange thickness ratio ( $\rho_t$ ) at different flange width ratios ( $\rho_b$ ) for  $\rho = 0.5$ ,  $f_c' = 30$  MPa &  $a/h = 2$ .

207

208

### 3.7. Effect of longitudinal steel in flange

209

210

211

212

213

The ultimate load predicted for T-beams with variable flange longitudinal reinforcement percentile ratios (0, 0.5, 1.0, and 2) is shown in Fig.13 for three cases of shear span to depth ratio ( $a/h = 0.5$ , 1.0, and 2.0). Figure 13 shows that increasing flange longitudinal reinforcement,  $\rho$ , from 0% to 2% increases the beam ultimate load by an average of 8%, 29%, and 27% for  $a/h = 0.5$ , 1.0, and 2; respectively.

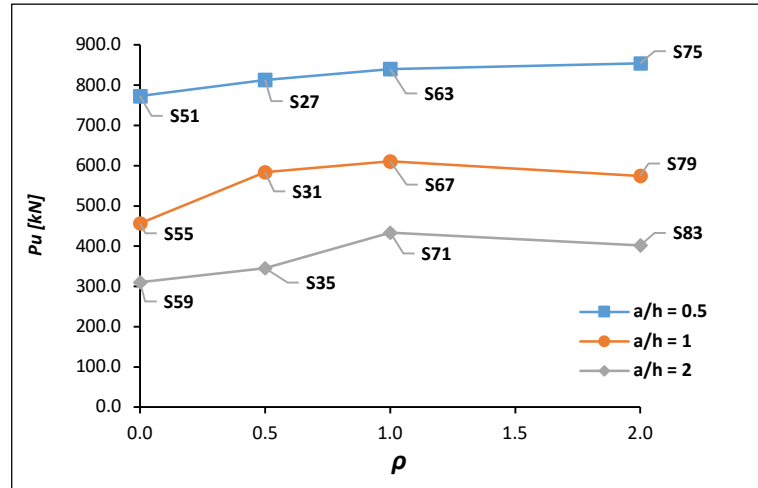


**Fig. 13** Effect of flange longitudinal reinforcement on Ultimate load for different shear span to depth ratios for  $\rho_b = 7$ ,  $\rho_t = 0.5$  &  $f_c' = 30$  MPa.

214  
215

### 3.8. Effect of shear span to depth ratio

216 Results for T-beams with different shear span to depth ratios ( $a/h = 0.5, 1$ , and  $2$ ) are shown in  
217 Figs. 14 and 15 for  $\rho_t = 0.3$  and  $\rho = 0.5$ .

218 Figure 14 presents variations of the ultimate shear strength with the shear span-to-depth ratio  
219 for  $\rho_b = 7$  and two values of concrete characteristic strength ( $f_c' = 30$  MPa and  $60$  MPa),  $\rho_t = 0.3$ ,  $\rho$   
220  $= 0.5$ ) and  $\rho_b = 7$ . For  $f_c' = 30$  MPa, Fig. 15 depicts variations of the ultimate shear strength with the  
221 shear span-to-depth ratio at various flange widths ( $\rho_b = 3, 5, 7$ , &  $9$ ). The increase in ( $a/h$ ) obviously  
222 reduced the shear capacity of flanged beams. In particular, decreasing the shear span to depth  
223 ratio from  $2.0$  to  $1.0$ , and then to  $0.5$  increased the ultimate shear strength by an average of  $49\%$   
224 and  $120\%$ , respectively. This trend is repeated for all flange widths and concrete strengths.

225 The load deflection curves for three T-beams that are identical but have different shear span to  
226 depth ratios ( $a/h = 0.5, 1.0$ , and  $2.0$ ) are presented in Fig.16. The curve indicates that the beam  
227 toughness ( $I$ ) is reduced as the shear span increases. Numerical values revealed that the  
228 toughness of beams having  $a/h$  of  $1.0$  and  $2.0$  were less than that of the similar beam with  $a/h$  of  
229  $0.5$  by about  $28\%$  and  $49\%$ , respectively.

230

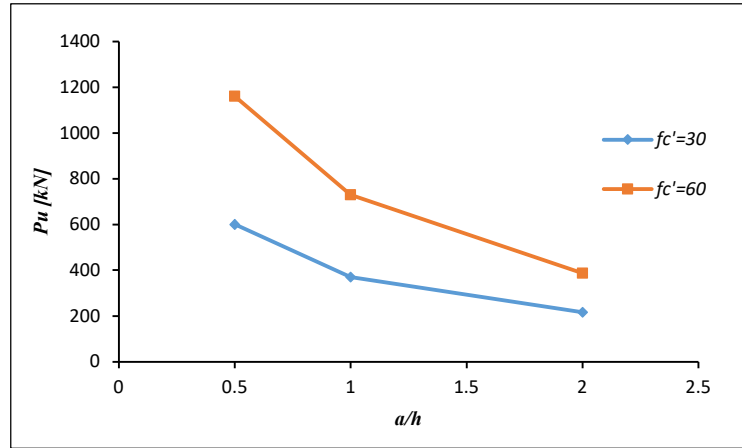


**Fig. 14** Effect of shear span-to-depth ratio on ultimate shear strength of T-beams for two values of concrete characteristic strength ( $\rho_b = 7$ ,  $\rho_t = 0.3$ ,  $\rho = 0.5$ ).

231  
232  
233  
234  
235  
236  
237  
238  
239

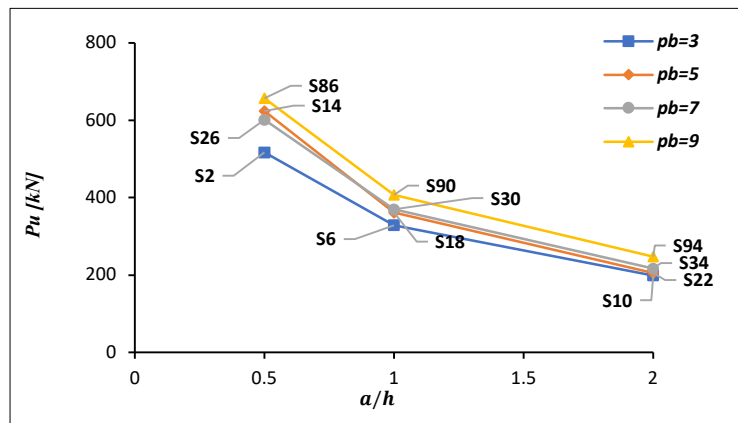


**Fig. 15** Effect of shear span-to-depth ratio on ultimate shear strength of T-beams with various flange widths ( $\rho_t = 0.3$ ,  $\rho = 0.5$  &  $f_c' = 30$  MPa).

242  
243  
244  
245  
246  
247  
248

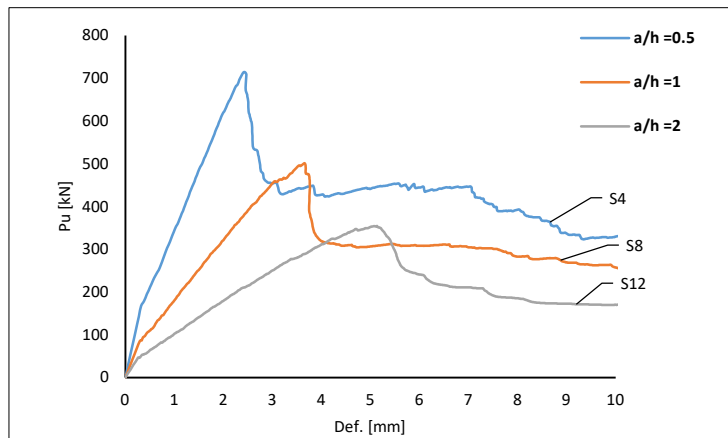


**Fig. 16** Effect of shear span-to-depth ratio on load-deflection curves of flanged beams ( $\rho_b = 3$ ,  $\rho_t = 0.7$ ,  $f_c' = 30$  MPa &  $\rho = 0.5$ ).

251  
252

### 3.9. Effect of concrete characteristic strength.

Values of the ultimate shear strengths calculated for 24 T-beams are displayed in Fig. 17. These values correspond to T-beams with one flange width  $\rho_b=7$ ; four values of flange thickness  $\rho_f=0.1, 0.3, 0.5$  &  $0.7$ ; and two values of concrete characteristic strengths ( $f_c'=30$  and  $60$ MPa). Study of data in Fig.17 and Table 3 showed that- on average- doubling concrete strength of beams results in doubling the first-yield load and increases the first-crack load by about 20%. The increase in beam ultimate shear capacity varies with both shear span and flange thickness. Numerically, doubling  $f_c'$  lead to shear capacity increases of 65%:99% for  $a/h=0.5$ ; 54%:97% for  $a/h=1$ ; and 27%:88% for  $a/h=2$ . It is also noted that the increase in shear capacity with increasing concrete strength becomes less pronounced as the span length or the flange thickness increases.

To examine the effect of concrete characteristic strength on beam toughness, the load-deflection relationship for beams with  $f_c'=30$  and  $60$ MPa are presented in Fig. 18 for three flange thickness ratios  $\rho_f=0.1, 0.3$  &  $0.7$  (other variables are  $\rho_b=7, a/h=0.5$ ). Considerable increase with an average of 74% in beam toughness,  $I$ , is observed with the increase in  $f_c'$  from 30 to 60 MPa. Finally, Fig.19 shows that the flexural crack pattern at failure is similar for beams with concrete strength of 30 to 60 MPa, while the use of higher concrete strength delayed the premature shear failure.

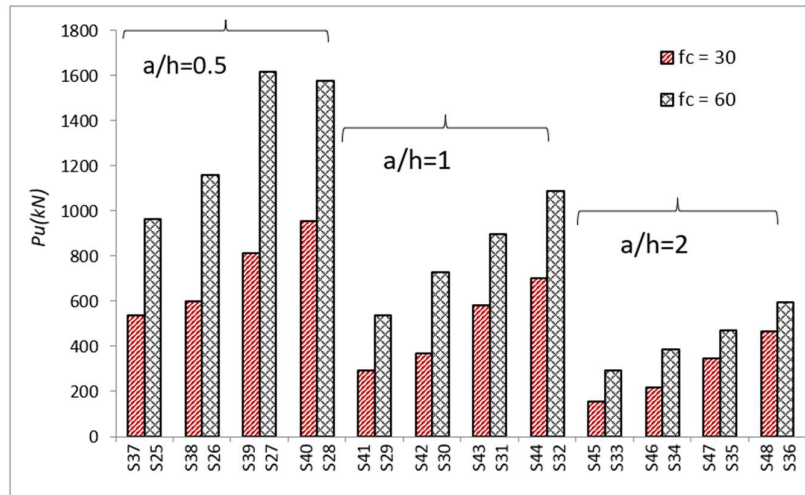


**Fig. 17** Effect of concrete characteristic strength on shear capacity for beams with variable shear span to depth ratios ( $\rho_b=7, \rho_f=0.1, 0.3, 0.5$  &  $0.7$ ).



316 and by 12% to 260% for  $(b_f/b_w) = 9$ . Thus, the effect of flange thickness is more pronounced. For  
 317 thin flanges ( $t/h = 0.10$ ), increasing flange width does not help.

318 3. Increasing flange longitudinal reinforcement,  $\rho$ , from 0% to 2% increased the beam ultimate load  
 319 by an average of 8%, 29%, and 27% for shear span to depth ratio ( $a/h$ ) of 0.5, 1.0, and 2;  
 320 respectively.

321 4. Investigation of the load deflection curves for identical T-beams that have different shear spans  
 322 indicated that the beam toughness ( $I$ ) decreases as the shear span increases. In particular, the  
 323 toughness of beams with  $a/h$  of 1.0 and 2.0 were less than that of the similar beam with  $a/h$  of  
 324 0.5 by about 28% and 49%, respectively.

325 5. Increasing the concrete characteristic strength  $f_c'$  from 30 to 60 MPa increased the beam shear  
 326 capacity by 65%:99% for  $a/h=0.5$ ; 54%:97% for  $a/h=1$ ; and 27%:88% for  $a/h=2$ .

327 6. The results of this study could help in reducing projects' cost by including the contribution of thick  
 328 compressed flanges to the shear strength of T-beams.

329

### 330 **References**

- 331 [1] ANSYS-Release Version 19.2.0., "A Finite Element Computer Software and User Manual for  
 332 Nonlinear Structural Analysis," ANSYS Inc. Canonsburg, PA 15317, 2018.
- 333 [2] Hesham A. A. and Wael M. M., "Shear behavior of reinforced lightweight concrete T-beams," Life  
 334 Science Journal, 16(8), 2019.
- 335 [3] Balamuralikrishnan R. and Saravanan J., "Finite Element Modelling of RC T - Beams Reinforced  
 336 Internally with GFRP Reinforcements," Civil Engineering Journal, 5(3), 2019.
- 337 [4] Hamdy K. S., Mohamed M. H., Mahmoud A. K. and Mahmoud Y. A. Z. "Finite Element Analysis on  
 338 the behavior of Strengthened RC Shallow T-Beams with Large Openings at Shear Zone Using CFRP  
 339 and BFRP sheets," IJSEAS, 3(11), 2017.
- 340 [5] Hugo C. B., Carlos C. and Manuel A.G., "A smeared Crack Analysis of Reinforced Concrete T-  
 341 Beams Strengthened with GFRP Composites," Engineering Structures 56, 2013: 1346-1361.
- 342 [6] Pansuk W and Sato Y., "Shear Mechanism Of Reinforcement Concrete T-Beams With Stirrups,"  
 343 Journal of Advanced Concrete Technology, 5(3), 2007: 395-408.
- 344 [7] Pansuk W., Sato Y., Takahashi R. and Ueda T., "Influence of Top Flange to Shear Capacity of  
 345 Reinforced Concrete T-Beams," Concrete Engineering Annual Papers, 26(2), 2004.
- 346 [8] Giaccio C., Al-Mahaidi R, and Taplin G., "Experimental study on the effect of flange geometry on the  
 347 shear strength of reinforced concrete T-beams subjected to concentrated loads," Can. J. Civ. Eng.  
 348 29,2002: 911-918
- 349 [9] Kachlakev D., and Miller T., "Finite Element Modeling of Reinforced Concrete Structures  
 350 Strengthened with FRP Laminates," Final Report, Oregon Department of Transportation, Salem,  
 351 Oregon, May 2001.
- 352 [10] Musmar M. A., Rjoub M. I. and Abdel Hadi M. A., "Nonlinear Finite Element Analysis of Shallow  
 353 Reinforced Concrete Beams Using SOLID65 Element," ARPJ Journal of Engineering and Applied  
 354 Sciences, 9(2), February 2014: 85-89
- 355 [11] Tjitradi D., Eliatun E. and Taufik S., "3D ANSYS Numerical Modeling of Reinforced Concrete Beam  
 356 Behavior under Different Collapsed Mechanisms," International Journal of Mechanics and Applications  
 357 2017, 7(1): 14-23

- 358 [12] Shah, S. P., Swartz, S. E., and Ouyang, C., "Fracture Mechanics of Concrete," John Wiley & Sons,  
359 Inc., New York, 1995.
- 360 [13] Bangash, M. Y. H., "Concrete and Concrete Structures: Numerical Modeling and Applications,"  
361 Elsevier Science Publishers Ltd., London, England, 1989.
- 362 [14] Gere, J. M. and Timoshenko, S. P., "Mechanics of Materials," PWS Publishing Company, Boston,  
363 Massachusetts, 1997.
- 364 [15] Kachlakev, D.I. and McCurry, D., Jr., "Simulated Full Scale Testing of Reinforced Concrete Beams  
365 Strengthened with FRP Composites: Experimental Results and Design Model Verification," Oregon  
366 Department of Transportation, Salem, Oregon, June 2000.
- 367 [16] Ramadan, O. M., Abdel-Kareem, A. H., El-Azab, I. A., & Abousafa, H. R., "Flange Contribution to  
368 the Shear Strength of RC T-Beams with Flange in Compression". Buildings 2022, 12(6): 803.
- 369 [17] ACI Committee 318., "Building Code Requirements for Structural Concrete ACI," vols. 318-14,  
370 2014.